

See discussions, stats, and author profiles for this publication at: <https://www.researchgate.net/publication/231648640>

# Chirality in Copper Nanoalloy Clusters

ARTICLE *in* THE JOURNAL OF PHYSICAL CHEMISTRY C · DECEMBER 2011

Impact Factor: 4.77 · DOI: 10.1021/jp209085r

---

CITATIONS

10

---

READS

12

4 AUTHORS, INCLUDING:



**Christian Krekeler**

Technische Universität Braunschweig

17 PUBLICATIONS 371 CITATIONS

SEE PROFILE





**David Avnir**

Hebrew University of Jerusalem

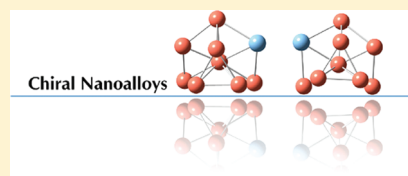
386 PUBLICATIONS 16,844 CITATIONS

SEE PROFILE

# Chirality in Copper Nanoalloy Clusters

Hadassah Elgavi,<sup>†</sup> Christian Krekeler,<sup>‡</sup> Robert Berger,<sup>\*,‡</sup> and David Avnir<sup>\*,†</sup><sup>†</sup>Institute of Chemistry and the Lise Meitner Research Center for Quantum Chemistry, The Hebrew University of Jerusalem, Jerusalem 91904, Israel<sup>‡</sup>Clemens-Schoepf Institute, Technical University of Darmstadt, Darmstadt D-64287, Germany Supporting Information  Web-Enhanced

**ABSTRACT:** It is shown that chirality is common in bimetallic clusters. Specifically, a detailed computational study of two copper clusters,  $\text{Cu}_n^+$  ( $n = 9, 11$ ), demonstrates that exchange of one copper atom with another metal atom (Ni, Zn, Ag, or Au) at various locations, leads, in most cases, to chirality in the a priori achiral cluster ( $n = 9$ ) and always preserves it in the a priori chiral one ( $n = 11$ ). Chirality was evaluated on a quantitative level, employing the Continuous Chirality Measure methodology, in two versions: a purely geometric structure analysis, and an analysis which takes into account the different nature of the atoms. Physical aspects of chirality were demonstrated by emergence of vibrational circular dichroism signals and by the emergence of parity violation (PV) energy difference, which is calculated by employing a quasi-relativistic approach. In the case of  $\text{AgCu}_{10}^+$  (p9), the PV energy splitting value is about  $\sim 10^{-15}$  Hartree, bringing this nanoalloy close to the range of systems that have been discussed as promising candidates for a measurement of this phenomenon on the molecular level.



## 1. INTRODUCTION

Metal clusters have drawn a great deal of attention due to their unique characteristics, including their optical properties,<sup>1</sup> magnetic properties,<sup>2</sup> catalytic reactivity,<sup>3,4</sup> and more; these often differ significantly from both the bulk and the single atom properties. A pertinent example is the catalytic activity of nanoparticles of gold, a feature not found in the bulk metal.<sup>3</sup> Nanodevices based on such properties have been described.<sup>5</sup> Whereas most of the research on metallic nanoclusters initially focused on pure metals, the wider horizons of metallic nanoalloys—metal clusters composed of more than one metal element—have begun to receive more attention.<sup>6–8</sup> Considering the fact that nanoalloys represent, in principle, endless combinations of the  $\sim 100$  metals, focusing on these intermetallic nanoparticles seems to carry a promise of a rich library of fine-tuned applications. Note that in this case, not only are the properties size-dependent, but they also depend on composition—the ratio between the two (or more) metals—and on the specific locations of the different atoms within a given cluster size; catalysis with alloys comes to mind as an interesting alternative to catalysis by pure metals, as examples abound.<sup>9–14</sup>

Here we focus on chirality in metal nanoparticles,<sup>15</sup> interest in which is based on their optical<sup>5</sup> and magneto-optical<sup>2</sup> properties, as well as on their potential use in enantioselective catalytic reactivity.<sup>4</sup> In the latter context, we mention that separation of chiral nanoparticles into pure enantiomers has been achieved.<sup>16,17</sup> The notion of a chiral metal might, however, appear counter-intuitive: after all, the close packing of metallic atoms (fcc, bcc, hcp), renders their crystal structure achiral as far as the unit cell is concerned. We note, however, that certain rare metal phases are known, for instance in tellurium,<sup>18</sup> where a helical structure renders the metal chiral, or in holmium,<sup>19</sup> where in a certain

phase the electron spins acquire a helical arrangement that results in chirality caused by the electronic structure. Chirality in the context of the more common metals exists in several ways: In cuts along specific Miller-indices which expose surface step patterns which are chiral;<sup>20,21</sup> in adsorption of chiral molecules on achiral low Miller-indices metallic surfaces, which distort the atoms array in a chiral manner;<sup>22</sup> in adsorption of complex organic molecules on metal surfaces;<sup>23</sup> and, recently, we have shown that chirality can be induced in metals by doping and imprinting.<sup>24,25</sup>

Small metal clusters have distinct structures—depending on size and on the involved atom—which are different from the crystal structure of the bulk metal, and which in many cases are achiral.<sup>26–29</sup> Examples of chiral single metal clusters have been mainly reported for gold.<sup>30–35</sup> Additional relevant reports to this study are the chiral bimetallic core-shell clusters;<sup>33</sup> the stable  $\text{Ni}_m\text{Ag}_n$  clusters, some of which are chiral (although this property is not mentioned there);<sup>34</sup> and the studies in which adsorption of chiral molecules on gold clusters induces chirality in their structure.<sup>30,36,37</sup>

Having in mind the richness of structures expected from nanoalloys, we explored the extent to which chirality might be abundant in the domain of metal clusters. Introducing a different metal atom in a pure metal cluster is likely to lower the symmetry of the cluster. This is expected, both due to the existence of a heteroatom in the structure and due to the different arrangement of bonds around the heteroatom. If lowering of the symmetry removes all improper symmetry elements, then chirality will emerge. Indeed, we show that chirality is abundant in nanoalloys,

Received: September 20, 2011

Revised: November 30, 2011

Published: December 01, 2011

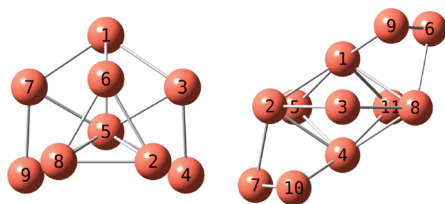


**Figure 1.** The optimized structures of the  $\text{Cu}_9^+$  (left) and  $\text{Cu}_{11}^+$  (right) clusters. The numbers label the atoms in each cluster; the homotops are identified by these labels. The  $\text{Cu}_9^+$  has  $C_5$  point group symmetry, the mirror plane passes through atoms 1, 5, and 6. The  $\text{Cu}_{11}^+$  has  $C_2$  point group symmetry, the rotation axis passes through atom 3 perpendicular to the page. 3D rotatable images in xyz format are available (see Image 1 and Image 2).

by far more than in single metal clusters. We determined the extent of this phenomenon by employing a quantitative measure of chirality, namely the Continuous Chirality Measure (CCM) methodology. We then continue to show that these chiral structures also display physical aspects of chirality by emergence of vibrational circular dichroism signals, and by the emergence of significant parity violating (PV) energy differences.

## 2. THE STUDIED CLUSTERS AND THE QUANTITATIVE COMPUTATIONAL METHODS

The selected clusters are nanoalloys based on  $\text{Cu}_n^+$  ( $n = 9, 11$ ); that is, one copper atom was substituted with another metal atom to construct  $\text{XCu}_{n-1}^m$  ( $X = \text{Ni, Zn, Ag or Au}$ ;  $m = 0$  or  $m = 1$  in order to get a closed shell configuration). Of the two initial clusters (Figure 1), the equilibrium structure of  $\text{Cu}_9^+$  is achiral and has  $C_5$  point group symmetry, while the  $\text{Cu}_{11}^+$  cluster has  $C_2$  symmetry, is chiral to begin with and was used as a comparative case to find out how does substitution affect, quantitatively, the already-existing chirality, and whether substitution in such case may decrease the degree of chirality. The copper atom substitution procedure results in many isomers or *homotops*. (The term “homotops”<sup>66</sup> is used to describe bimetallic clusters ( $\text{A}_a\text{B}_b$ ) which have a fixed number of atoms ( $a + b = N$ ), fixed composition ( $a/b$  ratio) and the same geometrical structure (prior to geometrical optimization) but differ in the arrangement of the unlike atoms.) The different homotops are marked in the following way:  $\text{XCu}_{n-1}^m\text{p}(i)$  where  $\text{p}(i)$  marks the position of the atom that was substituted (see Figure 1). In total, 48 nanoalloy structures based on both initial clusters were obtained (not including enantiomers).

The equilibrium structures of the clusters were obtained computationally. Structure optimizations and subsequent harmonic vibrational frequency calculations were performed based on density functional theory (DFT) with the hybrid functional B3P86 (which combines the Becke three-parameter hybrid exchange functional with the Perdew gradient-corrected correlation functional)<sup>38,39</sup> as implemented in the Gaussian03 program.<sup>40</sup> This functional has been chosen as it has been shown to give satisfactory results for coinage metals.<sup>41</sup> Energy consistent effective core potentials (ECP) together with their energy optimized contracted basis sets were used in order to incorporate relativistic effects and were chosen from the Stuttgart RSC 1997 ECP collection.<sup>42–45</sup> The initial pure metal cluster structures were obtained from the Cambridge Cluster Database (CCDB)<sup>46</sup> from ref 28. The initial step was energy optimization of these structures which was followed by harmonic vibrational frequency analyses,

in order to ensure that the obtained structures correspond to minima on the Born–Oppenheimer hyper-surface. The equilibrium structures of the alloys were obtained by the following process: First, one atom in an optimized pure metal cluster was replaced with an atom of a different metal. This configuration was then used as an initial structure for optimization in the same way the pure metal clusters were optimized. As some atoms are symmetry equivalent, there is not always a need to evaluate all the possible substitutions. In all of these calculations, the self-consistent field equations were solved for a singlet electronic state within the real restricted Kohn–Sham framework.

The degree of chirality of the clusters was determined by using the Continuous Chirality Measure (CCM) methodology. The main idea behind this approach is that chirality can be treated as a continuous (lack of symmetry) property rather than as a dichotomous one (chiral or not). The CCM is a distance function which measures how far a given structure is from achirality, i.e., from the closest object which has  $S_n$  point group symmetry ( $S_1 = C_s$  and  $n > 1$  is even). Hence, the chirality value would be zero for an achiral structure and the further the structure from improper symmetry the higher the CCM value.

Given an object specified by  $N$  vertices and the closest achiral object, the CCM is defined to be as follows:  $\text{CCM} = S(\text{G}_{\text{achiral}}) = \min\{S(S_1), S(S_2), S(S_4), \dots\}$

$$S_Q(\text{G}) = 100 \times \min \left[ \frac{\sum_{k=1}^N |\vec{q}_k - \vec{p}_k|^2}{\sum_{k=1}^N |\vec{q}_k - \vec{q}_0|^2} \right] \quad (1)$$

where  $q_k$  are the vertices of the investigated object and  $p_k$  are the vertices of the closest achiral object (which, as a special feature of this distance measure, is unknown a priori, but is obtained as an outcome of the computation). Finally,  $q_0$  corresponds to the coordinate vector of the center of the investigated structure  $q_k$ .

The measure is normalized by the root-mean-square size of the object  $Q$ . The factor 100 expands the scale for convenience, so that the value of the measure ranges from zero to an upper bound which is lower than 100 (the 100 limit is obtained in the more general Continuous Symmetry Measure<sup>47</sup>). For a more detailed description of the CCM computational methods see refs 47–50 for examples of its applications across chemistry see refs 51–54

For each cluster, two types of chirality measures were computed: one takes into account the identity of the elements in the cluster, that is, different elements are not interchangeable—we term this measure the *chirality measure*. The second is purely geometrical, namely it does not distinguish between different chemical elements, but measures of the amount of chirality due to the distortion of the geometric structure as a whole—we term this the *structural chirality measure*. For pure metal clusters, the measures are, of course, the same.

Vibrational circular dichroism (VCD) spectra were produced to ensure and demonstrate the physical chirality of the resulting enantiomeric pairs of nanoalloys. These were computed with the Gaussian03 program with the same density functional, basis set and effective core potential selected for optimization.

Parity violating potentials ( $V_{\text{PV}}$ ) as computed for the equilibrium structures are also reported. PV is a phenomenon related to the fundamental weak interaction. The weak force is not invariant under spatial inversion, in other words, it is chiral. As the

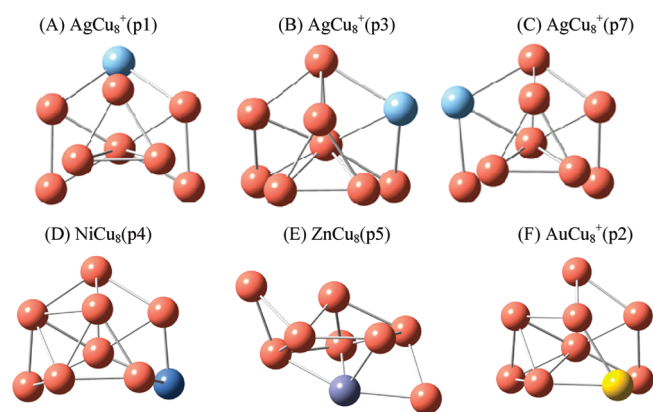


**Figure 2.** Representative nanoalloy structures; (A) an achiral homotop; (B) and (C) an enantiomeric pair of chiral nanoalloys; (D)–(F) Ni, Zn and Au homotops, accordingly.

**Table 1.** Values of the Chirality and Structural Chirality Measures for the Nanoalloys Obtained from the  $\text{Cu}_9^+$  Cluster

cluster	replaced atom <sup>a</sup>	chirality measure	structural chirality measure
$\text{Cu}_9^+$		0.00	0.00
$\text{NiCu}_8$	1	0.00	0.00
	2	4.19	0.02
	3	2.63	0.01
	4	2.54	0.04
	5	0.00	0.00
	6	0.00	0.00
$\text{ZnCu}_8$	1	0.00	0.00
	2	1.89	1.89
	3	0.00	0.00
	4	3.50	3.50
	5	1.60	1.60
	6	0.00	0.00
$\text{AgCu}_8^+$	1	0.00	0.00
	2	3.87	0.08
	3	3.13	0.11
	4	2.69	0.05
	5	0.00	0.00
	6	0.00	0.00
$\text{AuCu}_8^+$	1	0.00	0.00
	2	3.42	0.09
	3	3.50	0.17
	4	2.69	0.03
	5	0.00	0.00
	6	0.00	0.00

<sup>a</sup> The replaced atom refers to the position label of the substituted atom in the pure metal cluster.

weak interaction has specific handedness, molecular enantiomers are predicted to differ in their energy by a small amount,  $\Delta E_{\text{PV}}$ , which is approximately equal to two times  $V_{\text{PV}}$ . For achiral molecules, the effect should vanish.

To obtain the parity violating potential,  $V_{\text{PV}}$ , we used a modified quasi-relativistic (two-component) development version<sup>55,56</sup> of the quantum chemical program TURBOMOLE.<sup>57,58</sup> For each

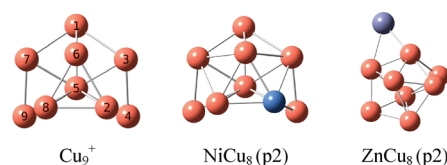


**Figure 3.** The  $\text{Cu}_9^+$  cluster and the Ni and Zn homotops for position #2. Clearly, the Ni alloy resembles the original structure as opposed to the Zn alloy.

structure a single point calculation of  $V_{\text{PV}}$  was carried out within the zeroth order regular approximation (ZORA), using two different density functionals (namely BLYP<sup>38,59</sup> and B3LYP<sup>38,59,60</sup> which have also been employed in other studies on  $V_{\text{PV}}$ ) as it is known from previous work (see, e.g., ref 61) that parity violating potentials can display a significant dependence on the selected functional. We have chosen all-electron even-tempered basis sets, including steep s- and p-functions to describe the parity violating operator and up to f- functions, according to previously studied systems.<sup>56</sup> In the first step, we performed a preoptimization of the orbitals within the efficiently implemented conventional non-relativistic scheme to obtain a starting guess for the following scalar relativistic calculation and the orbitals obtained therein as initial guess for the subsequent quasi-relativistic calculation to determine the  $V_{\text{PV}}$ .

### 3. CHIRALITY ANALYSIS OF THE CLUSTERS

The  $\text{XCu}_8^m$  clusters: We begin with the 24 clusters which are obtained from the achiral  $\text{Cu}_9^+$  cluster (not including enantiomers). Representative structures are shown in Figure 2, (for additional structures and information, refer to the Supporting Information). The chirality values for all homotops are collected in Table 1. It can be seen that half of the nanoalloys are chiral, and this is evident from both types of chirality measures. The chirality values vary from 0.01 to 4.19.

For  $X = \text{Ni}$ ,  $\text{Ag}$ , and  $\text{Au}$ , the homotops which are formed by substituting atoms number 1, 5, and 6 remain achiral, because these three atoms lie on the  $\text{Cu}_9^+$  cluster's mirror plane (Figure 1). The structural deformation due to substitution in these three positions is relatively minor and so the bimetallic clusters retain their symmetry plane. However, in the case of the  $\text{ZnCu}_8$  alloys, the initial geometrical structure (i.e., that of the  $\text{Cu}_9^+$  after substitution of one Cu for Zn) was less stable than in the other three alloys. Consequently, the structures of the  $\text{ZnCu}_8$  nanoalloys are considerably different (Figure 3). [These large changes in equilibrium structure are due to the fact that neutral  $\text{ZnCu}_8$  is not isoelectronic in the valence shell to the other nanoalloys studied herein. Indeed, for (valence) isoelectronic  $\text{ZnCu}_8^{2+}$  we obtain equilibrium structures which resemble those of the parent  $\text{Cu}_9^+$  (not shown here).]

Finally, as the nanoalloys with  $X = \text{Ni}$ ,  $\text{Ag}$ , and  $\text{Au}$  are similar in form to the original  $\text{Cu}_9^+$  structure, the purely geometrical chirality calculation yields values which are lower than the full calculation (which takes into account the chemical nature), in most cases by 2 orders of magnitude. The change in the overall shape of the clusters by substitution is illustrated by calculating the alloy's distance from the original metal cluster shape. According to the CSM methodology, we can determine the distance to a predetermined shape instead of evaluating the symmetry content. This shape measure is a distance function between the shape of the examined object and the selected



reference shape (disregarding the type of atom; for more information about this measure see refs 62, 63). In terms of eq 1,  $q_k$  are the vertices of the alloy and  $p_k$  are the vertices of the pure metal cluster and the shape measure equals  $S_Q$ . Shape measure values for  $\text{NiCu}_8(\text{p}3)$ ,  $\text{AgCu}_8^+(\text{p}3)$ , and  $\text{AuCu}_8^+(\text{p}3)$  are collected in Table 2 as representative examples. The shape measure values are around 0.2, similar in magnitude to the structural chirality measure, demonstrating once more that these clusters' chirality mainly due to the substitution and not their shape.

The  $\text{XCu}_{10}^m$  clusters: In order to investigate how existing chirality in a pure metal cluster is affected by alloying, we studied the chiral  $\text{Cu}_{11}^+$  (CCM of 3.01) in the same way. We find that the degree of chirality does not vary significantly, and CCM values, ranging from 2.6 to 3.4, were obtained. Table 3 collects the results for one of the homotops (the full table can be found in the Supporting Information) and Figure 4 provides several examples. It is seen that alloying preserves here the initial chirality, and we attribute this observation to the fact that the original  $C_2$  symmetry of the  $\text{Cu}_{11}^+$  cluster, which is the main source of its chirality, is almost retained upon substitution. How far each of the homotops is from  $C_2$  symmetry can be quantified using the continuous symmetry measure (CSM). The CSM is the parent concept to the CCM and is a function of the distance from the closest symmetric object.<sup>64</sup> The value of the symmetry measure is calculated

**Table 2. Values of the Chirality, Structural Chirality and Shape Measures for  $\text{Cu}_9^+$  Alloys**

cluster	shape measure	structural chirality	
		measure	chirality measure
$\text{NiCu}_8(\text{p}3)$	0.18	0.01	2.63
$\text{AgCu}_8^+(\text{p}3)$	0.29	0.11	3.13
$\text{AuCu}_8^+(\text{p}3)$	0.32	0.17	3.50

**Table 3. Values of the Structural  $C_2$  Symmetry Measures and the Chirality and Structural Chirality Measures for  $\text{AuCu}_{10}^+$  Nanoalloys**

replaced atom in $\text{Cu}_{11}^+$	chirality measure	structural chirality measure	$S(C_2)$ : structural $C_2$ measure
	3.01	3.01	0.00
1	2.90	2.60	0.14
2	3.11	2.89	0.09
3	3.23	2.97	0.00
5	3.11	3.11	0.03
6	2.77	2.77	0.05
9	2.83	2.83	0.10

from eq 1, where  $G$  is  $C_2$ . As can be seen in Table 3 for the  $\text{AuCu}_{10}^+$  homotops, the value of the structural  $S(C_2)$

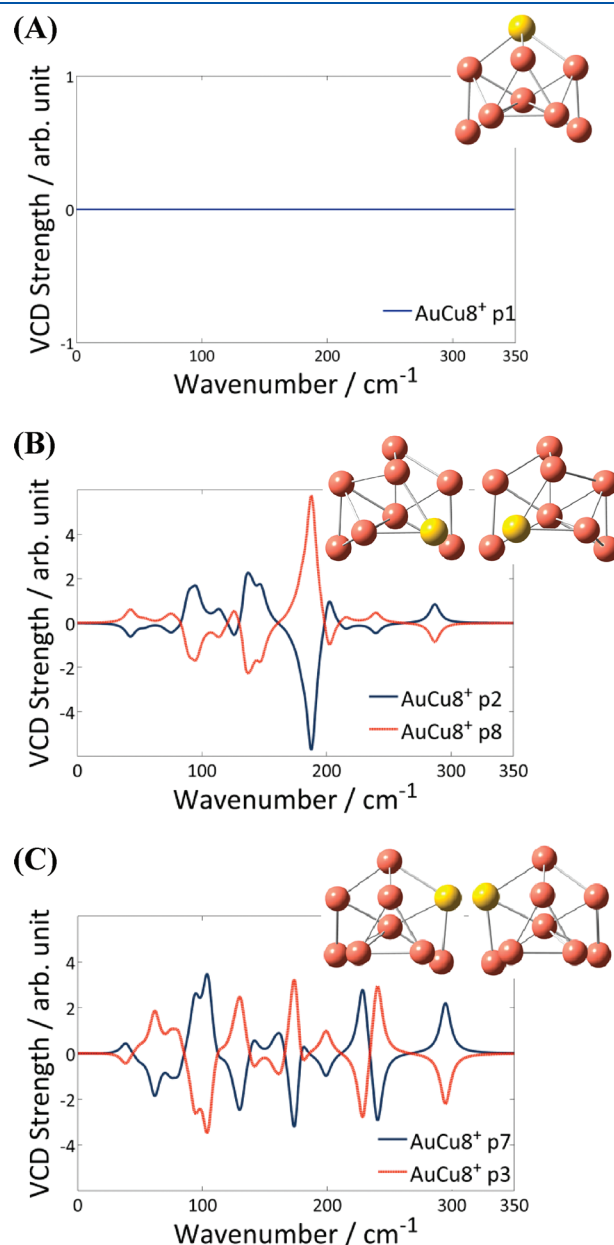


**Figure 5.** VCD spectra for several  $\text{AuCu}_8^+$  clusters. (A) For the achiral  $\text{AuCu}_8^+(\text{p}1)$  the VCD strength is zero, as expected. (B) and (C) show the spectra for two pairs of enantiomers,  $\text{AuCu}_8^+(\text{p}2)$  and  $(\text{p}8)$ , and  $\text{AuCu}_8^+(\text{p}3)$  and  $(\text{p}7)$ . In each case the enantiomers provide exact mirror image spectral lines.

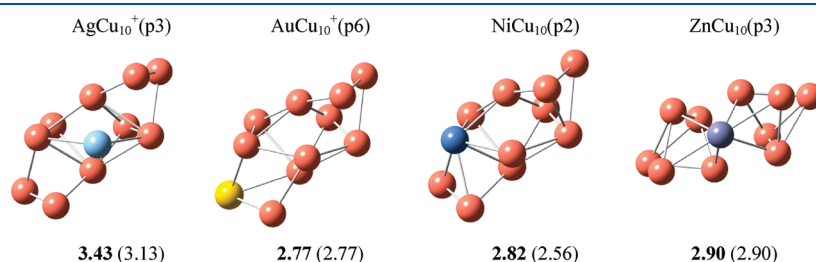


**Figure 4.** Examples of  $\text{XCu}_{10}^m$  nanoalloys; below each are their chirality measures (in bold) and the structural chirality measures (in brackets).

**Table 4.** Chirality Values and Parity Violating Potential  $V_{PV}$ <sup>a</sup>

cluster	chirality measure	structural	$V_{PV}$ (BLYP)/ $E_h$	$V_{PV}$ (B3LYP)/ $E_h$
		chirality measure		
$Cu_9^+$	0.00	0.00	$(8.8 \times 10^{-22})$	$(1.9 \times 10^{-22})$
$Cu_{11}^+$	3.01	3.01	$-1.5 \times 10^{-17}$	$-1.1 \times 10^{-16}$
$NiCu_{10}$ (p1)	3.00	3.00	$-5.2 \times 10^{-16}$	$-4.0 \times 10^{-16}$
$ZnCu_8$ (p2)	1.89	1.89	$-6.1 \times 10^{-17}$	$-3.7 \times 10^{-17}$
$ZnCu_8$ (p4)	3.50	3.50	$-1.5 \times 10^{-18}$	$-6.1 \times 10^{-18}$
$ZnCu_8$ (p5)	1.60	1.60	$-6.4 \times 10^{-17}$	$-5.9 \times 10^{-17}$
$ZnCu_{10}$ (p6)	3.00	3.00	$7.0 \times 10^{-17}$	$5.1 \times 10^{-17}$
$AgCu_8^+$ (p1)	0.00	0.00	$(-8.1 \times 10^{-22})$	$(2.6 \times 10^{-22})$
$AgCu_8^+$ (p2)	3.87	0.08	$3.5 \times 10^{-16}$	$3.5 \times 10^{-16}$
$AgCu_8^+$ (p3)	3.13	0.11	$-4.9 \times 10^{-16}$	$-4.0 \times 10^{-16}$
$AgCu_8^+$ (p4)	2.69	0.05	$-1.7 \times 10^{-17}$	$2.9 \times 10^{-17}$
$AgCu_{10}^+$ (p9)	3.11	2.97	$-1.3 \times 10^{-15}$	$-1.4 \times 10^{-15}$

<sup>a</sup> Values in parentheses indicate a numerical value.

(i.e., ignoring the atom type labeling) is low, indicating that the structures are very close to  $C_2$  symmetry.

#### 4. COMPUTED PHYSICAL PROPERTIES RELATED TO THE CHIRALITY OF THE CLUSTERS

Next, it was interesting to test whether the structural chirality of the clusters shows up in chirality-induced properties. We selected two physical properties, one a classical test—VCD spectra, and the other a still elusive observation on the molecular level, namely the PV energy splitting ( $\Delta E_{PV}$ ).

**4.1. Vibrational Circular Dichroism.** In addition to demonstrating a chirality-related physical property of the clusters, the VCD analyses served also as tests for the authenticity of the computation results. The spectrum of the achiral  $AuCu_8^+$  is presented in Figure 5(A) and shows, as expected, zero optical activity. In contrast, the VCD spectra are definitely pronounced for the two pairs of enantiomers— $AuCu_8^+$ (p2) and (p8) and  $AuCu_8^+$ (p3) and (p7) and, as seen in and Figure 5(B) and (C), each pair of enantiomers provides exact mirror image spectral lines confirming that these are indeed enantiomers.

**4.2. Parity Violation Energy Splitting.** Due to the chirality of the weak interaction, enantiomers are predicted to differ minutely in their energy. Though the effect is small, of the order of  $10^{-18}$  Hartree (corresponding to pJ mol<sup>-1</sup>), theory shows that PV is important for the understanding of chirality in molecular physics.<sup>65</sup> We calculated the PV potentials for a selection of the copper based clusters which have shown values different from zero in the CCM analysis approach. The results are collected in Table 4. A positive (negative) value for the parity violating potential indicates that the given enantiomer is about  $|2V_{PV}|$  higher (lower) in energy than its mirror image.

The  $V_{PV}$  for chiral clusters are between 5 to 7 orders of magnitude larger than the computational inaccuracy, as represented in the values of the achiral  $Cu_9^+$  and  $AgCu_8^+$ (p1) clusters. The choice of density functional affects the results of the nanoalloys studied herein within some 30%. For two nanoalloys,  $ZnCu_8$  (p2) and  $AgCu_8^+$  (p4), stronger relative changes are observed with  $V_{PV}$  changing sign for  $AgCu_8^+$  (p4) upon change of functional but being small in magnitude as compared to  $V_{PV}$  of

the other silver containing nanoalloys. Here more sophisticated electronic structure approaches would be required. The largest calculated absolute  $V_{PV}$  value is for the  $AgCu_{10}^+$ (p9) cluster ( $\sim 1 \times 10^{-15}$  Hartree), on the same order of magnitude as the one computed for the hypothetical molecule CHAtFI that was considered to be among those molecules showing a particularly large PV effect (see ref 61.).

#### 5. CONCLUSIONS

To summarize, equilibrium structures were computed for 48 nanoalloys based on two pure copper clusters:  $Cu_{11}^+$  and  $Cu_9^+$ . The chirality of the clusters was evaluated using the CCM method; 36 of these alloys are found to be chiral. Computations of VCD spectra confirmed the chirality of the resulting homotops and it was shown that the chirality of the nanoalloys gives rise to appreciable  $V_{PV}$ . The main message emerging from this study is that when chirality in metal clusters is of interest, the world of metallic alloys offers by far a richer library than the pure metals, which have been the focus of metal chirality studies so far. Since the properties of nanoalloys are affected by their composition, alloying may be used to design and fine-tune cluster specific desirable properties while preserving their chiral characteristics.

#### ■ ASSOCIATED CONTENT

**S Supporting Information.** Energies, chirality measure values, and images of all nanoalloy structures; Chirality and structural chirality measure values for all  $XCu_{10}^m$  nanoalloys. This material is available free of charge via the Internet at <http://pubs.acs.org>.

**W Web Enhanced Feature.** 3D rotatable images in xyz format.

#### ■ AUTHOR INFORMATION

##### Corresponding Author

\*Phone: +49 6151 16 3576; Fax: +49 6151 16 5591; E-mail: [robert.berger@tu-darmstadt.de](mailto:robert.berger@tu-darmstadt.de) (R.B.). Phone: +972-2-6585332; Fax: +972-2-6520099; E-mail: [david@chem.ch.huji.ac.il](mailto:david@chem.ch.huji.ac.il) (D.A.).

#### ■ ACKNOWLEDGMENT

The authors thank Dr. David Danovich, Dr. Chaim Dryzun, and Amir Zait for their assistance. This research was supported by a grant from the G.I.F., the German-Israeli Foundation for Scientific Research and Development.

#### ■ REFERENCES

- (1) Baev, A.; Samoc, M.; Prasad, P. N.; Krykunov, M.; Autschbach, J. *Opt. Express* **2007**, *15*, 5730.
- (2) Fromen, M. C.; Morillo, J.; Casanove, M. J.; Lecante, P. *Europhys. Lett.* **2006**, *73*, 885–891.
- (3) Haruta, M. *Catal. Today* **1997**, *36*, 153–166.
- (4) Szöllősi, G.; Mastalir, Á.; Király, Z.; Dékány, I. *J. Mater. Chem* **2005**, *15*, 2464.
- (5) Schmid, G.; Bäuml, M.; Geerkens, M.; Heim, I.; Osemann, C.; Sawitowski, T. *Chem. Soc. Rev.* **1999**, *28*, 179–185.
- (6) Bracey, C. L.; Ellis, P. R.; Hutchings, G. J. *Chem. Soc. Rev.* **2009**, *38*, 2231–2243.
- (7) Ferrando, R.; Jellinek, J.; Johnston, R. L. *Chem. Rev.* **2008**, *108*, 845–910.
- (8) Jellinek, J. *Faraday Discuss.* **2008**, *138*, 11.
- (9) Mukerjee, S.; Srinivasan, S. *J. Electroanal. Chem.* **1993**, *357*, 201–224.

- (10) Raghuveer, V.; Manthiram, A.; Bard, A. J. *J. Phys. Chem. B* **2005**, *109*, 22909–22912.
- (11) Stamenkovic, V. R.; Mun, B. S.; Arenz, M.; Mayrhofer, K. J. J.; Lucas, C. A.; Wang, G.; Ross, P. N.; Markovic, N. M. *Nat. Mater.* **2007**, *6*, 241–247.
- (12) Mazumder, V.; Chi, M.; More, K. L.; Sun, S. J. *Am. Chem. Soc.* **2010**, *132*, 7848–7849.
- (13) Koszinowski, K.; Schröder, D.; Schwarz, H. *J. Am. Chem. Soc.* **2003**, *125*, 3676–3677.
- (14) Koszinowski, K.; Schröder, D.; Schwarz, H. *Chemphyschem* **2003**, *4*, 1233–1237.
- (15) Zhang, J.; Albelda, M. T.; Liu, Y.; Canary, J. W. *Chirality* **2005**, *17*, 404–420.
- (16) Ward, T. J.; Baker, B. A. *Anal. Chem.* **2008**, *80*, 4363–4372.
- (17) Peng, X.; Komatsu, N.; Bhattacharya, S.; Shimawaki, T.; Aonuma, S.; Kimura, T.; Osuka, A. *Nat. Nanotechnol.* **2007**, *2*, 361–365.
- (18) Ghosh, P.; Bhattacharjee, J.; Waghmare, U. V. *J. Phys. Chem. C* **2008**, *112*, 983–989.
- (19) Achiwa, N.; Kawano, S.; Onodera, A.; Nakai, Y. *J. Phys. Colloq.* **1988**, *49*, C8-349–C8-350.
- (20) Baber, A. E.; Gellman, A. J.; Sholl, D. S.; Sykes, E. C. H. *J. Phys. Chem. C* **2008**, *112*, 11086–11089.
- (21) Sholl, D. S.; Gellman, A. J. *AIChE J.* **2009**, *55*, 2484–2490.
- (22) Kühnle, A.; Linderth, T. R.; Hammer, B.; Besenbacher, F. *Nature* **2002**, *415*, 891–893.
- (23) Barlow, S. M.; Raval, R. *Surf. Sci. Rep.* **2003**, *50*, 201–341.
- (24) Behar-Levy, H.; Neumann, O.; Naaman, R.; Avnir, D. *Adv. Mater.* **2007**, *19*, 1207–1211.
- (25) Durán Pachón, L.; Yosef, I.; Markus, T. Z.; Naaman, R.; Avnir, D.; Rothenberg, G. *Nat. Chem.* **2009**, *1*, 160–164.
- (26) Baletto, F.; Ferrando, R. *Rev. Mod. Phys.* **2005**, *77*, 371–423.
- (27) Calaminici, P.; Köster, A. M.; Russo, N.; Salahub, D. R. *J. Chem. Phys.* **1996**, *105*, 9546.
- (28) Fernández, E.; Soler, J.; Garzón, I.; Balbás, L. *Phys. Rev. B* **2004**, *70*, 165403.
- (29) Kabir, M.; Mookerjee, A.; Bhattacharya, A. *Phys. Rev. A* **2004**, *69*, 043203.
- (30) Garzón, I.; Reyes-Nava, J.; Rodríguez-Hernández, J.; Sigal, I.; Beltrán, M.; Michaelian, K. *Phys. Rev. B* **2002**, *66*, 1–4.
- (31) Jalbout, A. F.; Contreras-Torres, F. F.; Pérez, L. A.; Garzón, I. L. *J. Phys. Chem. A* **2008**, *112*, 353–7.
- (32) Lechtken, A.; Schooss, D.; Stairs, J. R.; Blom, M. N.; Furche, F.; Morgner, N.; Kostko, O.; Issendorff, B.; von; Kappes, M. M. *Angew. Chem., Int. Ed. Engl.* **2007**, *46*, 2944–8.
- (33) Gu, X.; Bulusu, S.; Li, X.; Zeng, X. C.; Li, J.; Gong, X. G.; Wang, L.-S. *J. Phys. Chem. C* **2007**, *111*, 8228–8232.
- (34) Santizo, I. E.; Hidalgo, F.; Pérez, L. A.; Noguez, C.; Garzón, I. L. *J. Phys. Chem. C* **2008**, *112*, 17533–17539.
- (35) Karttunen, A. J.; Linnolahti, M.; Pakkanen, T. A.; Pyykkö, P. *Chem. Commun. (Camb.)* **2008**, 465–467.
- (36) Gautier, C.; Bürgi, T. *J. Am. Chem. Soc.* **2006**, *128*, 11079–11087.
- (37) Gautier, C.; Bürgi, T. *J. Am. Chem. Soc.* **2008**, *130*, 7077–7084.
- (38) Becke, A. D. *J. Chem. Phys.* **1993**, *99*, 5648.
- (39) Perdew, J. P. *Phys. Rev. B* **1986**, *33*, 8822.
- (40) Frisch, M. J.; Trucks, G. W.; Schlegel, H. B.; Scuseria, G. E.; Robb, M. A.; Cheeseman, J. R.; Montgomery, Jr., J. A.; Vreven, T.; Kudin, K. N.; Burant, J. C.; Millam, J. M.; Iyengar, S. S.; Tomasi, J.; Barone, V.; Mennucci, B.; Cossi, M.; Scalmani, G.; Rega, N.; Petersson, G. A.; Nakatsuji, H.; Hada, M.; Ehara, M.; Toyota, K.; Fukuda, R.; Hasegawa, J.; Ishida, M.; Nakajima, T.; Honda, Y.; Kitao, O.; Nakai, H.; Klene, M.; Li, X.; Knox, J. E.; Hratchian, H. P.; Cross, J. B.; Bakken, V.; Adamo, C.; Jaramillo, J.; Gomperts, R.; Stratmann, R. E.; Yazyev, O.; Austin, A. J.; Cammi, R.; Pomelli, C.; Ochterski, J. W.; Ayala, P. Y.; Morokuma, K.; Voth, G. A.; Salvador, P.; Dannenberg, J. J.; Zakrzewski, V. G.; Dapprich, S.; Daniels, A. D.; Strain, M. C.; Farkas, O.; Malick, D. K.; Rabuck, A. D.; Raghavachari, K.; Foresman, J. B.; Ortiz, J. V.; Cui, Q.; Baboul, A. G.; Clifford, S.; Cioslowski, J.; Stefanov, B. B.; Liu, G.; Liashenko, A.; Piskorz, P.; Komaromi, I.; Martin, R. L.; Fox, D. J.; Keith, T.; Al-Laham, M. A.; Peng, C. Y.; Nanayakkara, A.; Challacombe, M.; Gill, P. M. W.; Johnson, B.; Chen, W.; Wong, M. W.; Gonzalez, C.; Pople, J. A. *Gaussian 03*, Revision D.01, 2004, Gaussian, Inc.: Wallingford, CT.
- (41) Visser, S. P.; de; Kumar, D.; Danovich, M.; Nevo, N.; Danovich, D.; Sharma, P. K.; Wu, W.; Shaik, S. *J. Phys. Chem. A* **2006**, *110*, 8510–8518.
- (42) Dolg, M.; Wedig, U.; Stoll, H.; Preuss, H. *J. Chem. Phys.* **1987**, *86*, 866.
- (43) Andrae, D.; Häußermann, U.; Dolg, M.; Stoll, H.; Preuß, H. *Theor. Chim. Acta* **1990**, *77*, 123–141.
- (44) Feller, D. *J. Comput. Chem.* **1996**, *17*, 1571–1586.
- (45) Schuchardt, K. L.; Didier, B. T.; Elsethagen, T.; Sun, L.; Gurumoorthi, V.; Chase, J.; Li, J.; Windus, T. L. *J. Chem. Inf. Model* **2007**, *47*, 1045–1052.
- (46) Wales, D. J.; Doyle, J. P. K.; Dullweber, A.; Hodges, M. P.; Naumkin, F. Y.; Calvo, F.; Hernandez-Rojas, J.; Middleton, T. F. The Cambridge Cluster Database <http://www.wales.cam.ac.uk/CCD.html>.
- (47) Dryzun, C.; Avnir, D. *Phys. Chem. Chem. Phys.* **2009**, *11*, 9653–9666.
- (48) Zabrodsky, H.; Avnir, D. *J. Am. Chem. Soc.* **1995**, *117*, 462–473.
- (49) Dryzun, C.; Avnir, D. *Chemphyschem* **2011**, *12*, 197–205.
- (50) Zayit, B.; Pinsky, M.; Elgavi, H.; Dryzun, C.; Avnir, D. *Chirality* **2011**, *23*, 17–23.
- (51) Ok, K. M.; Chi, E. O.; Halasyamani, P. S. *Chem. Soc. Rev.* **2006**, *35*, 710–717.
- (52) Jenkins, D. M.; Peters, J. C. *J. Am. Chem. Soc.* **2005**, *127*, 7148–7165.
- (53) Dryzun, C.; Mastai, Y.; Shvalb, A.; Avnir, D. *J. Mater. Chem* **2009**, *19*, 2062.
- (54) Breuer, J.; Avnir, D. *J. Chem. Phys.* **2005**, *122*, 074110.
- (55) Berger, R.; Langermann, N.; van Wüllen, C. *Phys. Rev. A* **2005**, *71*, 042105.
- (56) Berger, R.; Wüllen, C. van *J. Chem. Phys.* **2005**, *122*, 134316.
- (57) Ahlrichs, R.; Bar, M.; Haser, M.; Horn, H.; Kolmel, C. *Chem. Phys. Lett.* **1989**, *162*, 165–169.
- (58) Häser, M.; Ahlrichs, R. *J. Comput. Chem.* **1989**, *10*, 104–111.
- (59) Lee, C.; Yang, W.; Parr, R. G. *Phys. Rev. B* **1988**, *37*, 785–789.
- (60) Stephens, P. J.; Devlin, F. J.; Chabalowski, C. F.; Frisch, M. J. *J. Phys. Chem.* **1994**, *98*, 11623–11627.
- (61) Berger, R.; Stuber, J. L. *Mol. Phys.* **2007**, *105*, 41–49.
- (62) Pinsky, M.; Avnir, D. *Inorg. Chem.* **1998**, *37*, 5575–5582.
- (63) Pinsky, M.; Lipkowitz, K. B. K. B.; Avnir, D. *J. Math. Chem.* **2001**, *30*, 109–120.
- (64) Zabrodsky, H.; Peleg, S.; Avnir, D. *J. Am. Chem. Soc.* **1992**, *114*, 7843–7851.
- (65) Quack, M. *Angew. Chem., Int. Ed. Engl.* **2002**, *41*, 4618–4630.
- (66) Jellinek, J.; E.B., K. *Chem. Phys. Lett.* **1996**, *258*, 283–292.

## Supporting Information:

### Chirality in Copper Nanoalloy Clusters

*Hadassah Elgavi<sup>a</sup>, Christian Krekeler<sup>b</sup>, Robert Berger<sup>\*b</sup>, and David Avnir<sup>\*a</sup>*

<sup>a</sup> Institute of Chemistry and the Lise Meitner Research Center for Quantum Chemistry, The Hebrew University of Jerusalem, Jerusalem 91904, Israel; and

<sup>b</sup> Clemens-Schoepf Institute, Technical University of Darmstadt, Darmstadt D-64287, Germany

The binding energy (BE) of each of the clusters is given relative to the complete dissociation energy and is a measure of their stability. The BE is defined as:

$$BE = \Delta E_{dissc.} = (n - 1) \cdot E(Cu) + E(X) - E(cluster)$$

where  $n$  is the number of atoms in the cluster ( $n = 9, 11$ ) and  $E(X)$  denotes the energy of the substituent ( $X = Zn, Ni, Ag, Au$ ).

The full results for the  $Cu_{11}^+$  homotops, including both types of chirality measures (one of the geometric structure alone and the other taking the difference in atom types into account), are presented in Table 1 (results for the  $Cu_9^+$  homotops are given in the article). The structures of all the resulting nanoalloys are presented in Figure 1 and Figure 2.



**Table 1:** Values of the chirality and structural chirality measures of all nanoalloys obtained from the  $\text{Cu}_{11}^+$  cluster. The replaced atom refers to the label of the position of the substituted atom in the pure metal cluster.

Cluster	Replaced atom <sup>a</sup>	Chirality measure	Structural chirality measure
$\text{Cu}_{11}^+$	-	3.01	3.01
$\text{NiCu}_{10}$	1	3.00	3.00
	2	2.82	2.56
	3	2.93	2.93
	5	2.80	2.80
	6	2.66	2.66
	9	2.99	2.59
$\text{ZnCu}_{10}$	1	2.83	2.76
	2	3.31	2.95
	3	2.90	2.90
	5	3.11	3.08
	6	3.00	3.00
	9	3.27	3.14
$\text{AgCu}_{10}^+$	1	2.87	2.37
	2	3.12	2.98
	3	3.43	3.13
	5	3.12	3.12
	6	2.95	2.95
	9	3.11	2.97
$\text{AuCu}_{10}^+$	1	2.90	2.60
	2	3.11	2.89
	3	3.23	2.97
	5	3.11	3.11
	6	2.77	2.77
	9	2.83	2.83

<sup>a</sup> The replaced atom refers to the position label of the substituted atom in the pure metal cluster.

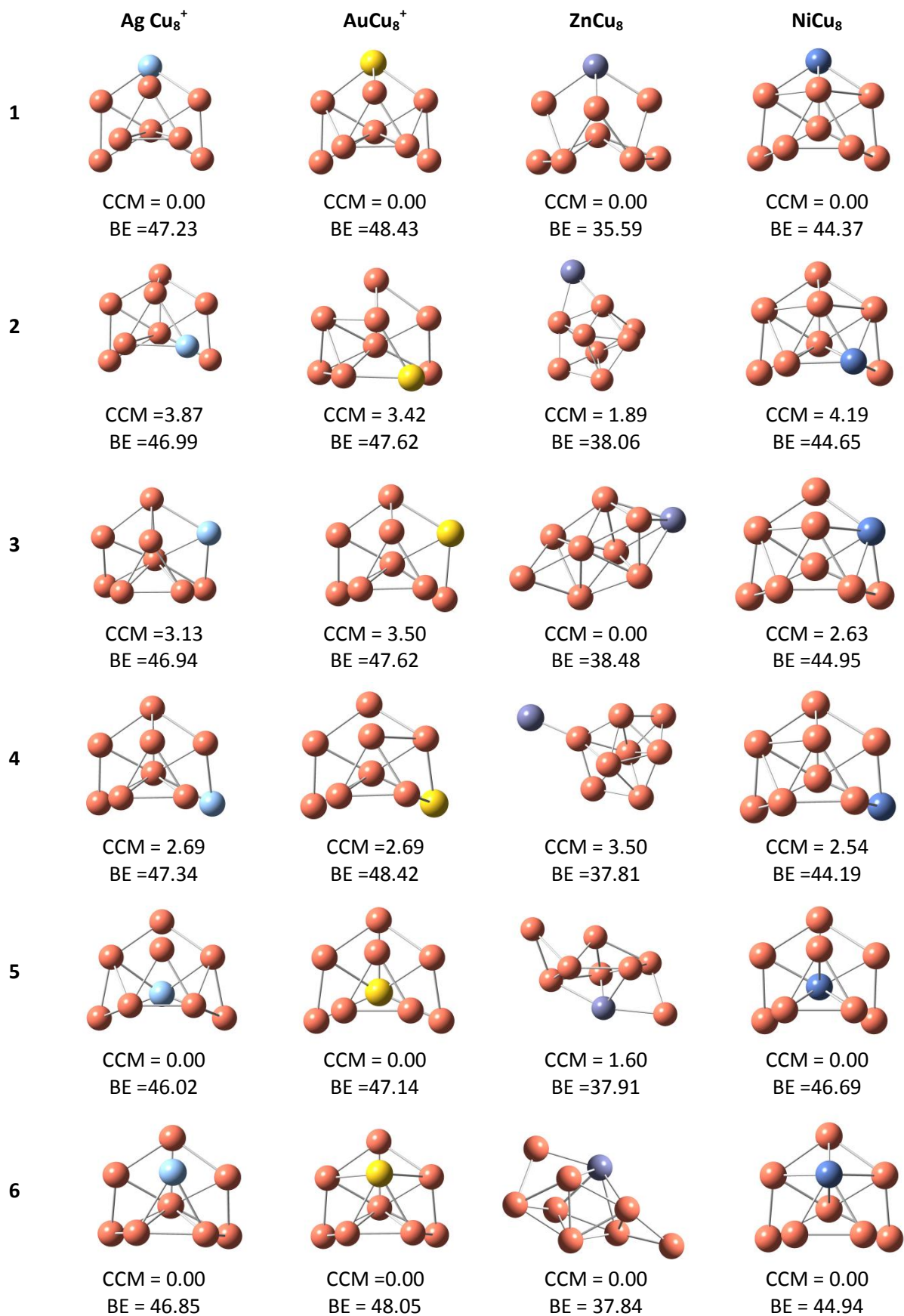


**Figure 1:** All resulting structures from the Cu<sub>9</sub><sup>+</sup> cluster. Each column shows the homotops for each alloy. The rows denote the label of the homotop (i.e. which atom was substituted). For each one, the CCM and binding energy (BE) per atom (in kcal/mol) are given.

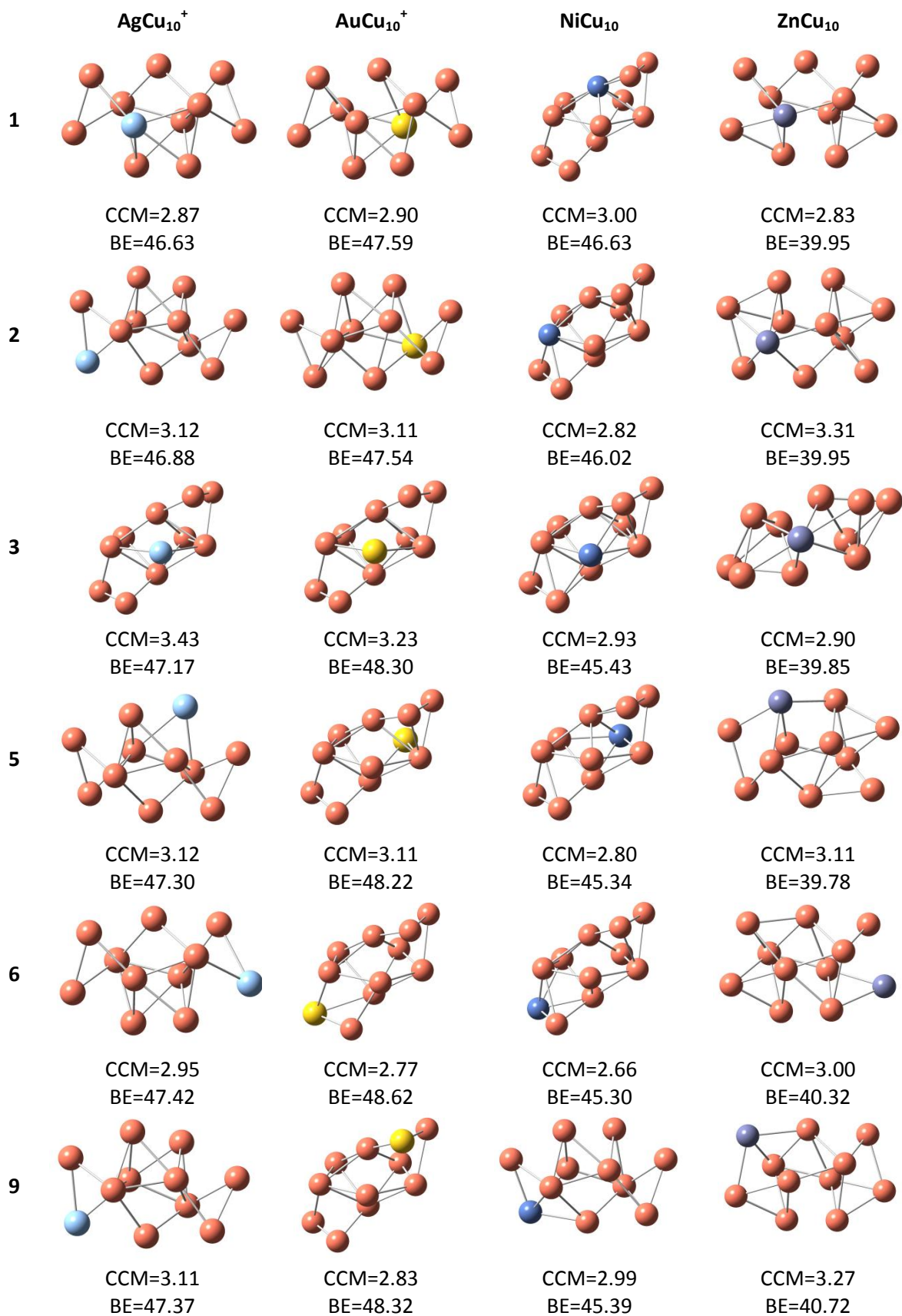


**Figure 2:** All resulting structures from the Cu<sub>11</sub><sup>+</sup> cluster. Each column shows the homotops for each alloy. The rows denote the label of the homotop (i.e. which atom was substituted). For each one, the CCM and binding energy (BE) per atom (in kcal/mol) are given